Three-dimensional spin-dependent dynamics in linearly polarized standing-wave fields

Yongsheng Fu,[1,2,*] Yu Liu,[1] Chunhui Wang,[1] Jiaolong Zeng,[1,2,†] and Jianmin Yuan[1,2,‡]
[1]*Department of Physics, National University of Defense Technology, Changsha 410073, China*
[2]*Department of Physics, Graduate School of China Academy of Engineering Physics, Beijing 100193, China*

(Received 29 August 2018; revised manuscript received 27 April 2019; published 10 July 2019)

There is a revival of the problem of how a relativistic particle with spin moves through an electromagnetic field. Our paper focuses on the spin-dependent dynamics of electrons in linearly polarized laser fields based on the Dirac equation and a classical spin model. It is proved that an electron at rest undergoes a three-dimensional motion moving out of the polarization-propagation plane when the initial spin is perpendicular to the magnetic field. We make a comprehensive investigation of the dynamics of quantum wave packets and classical electrons in both plane-wave and standing-wave fields. The wave packet travels in accordance with its center of mass in a plane-wave field but spreads heavily in a standing-wave field. The ensembles of classical electrons turn out to well simulate the quantum wave-packet dynamics in the standing-wave fields. We give the extended calculations of the electron dynamics with spin in the standing-wave field in the chaotic regime and find the quantum correspondence to the classical chaotic dynamics.

DOI: 10.1103/PhysRevA.100.013405

I. INTRODUCTION

Spin was proposed [1] originally as a concept to explain the Stern-Gerlach experiment [2] but accepted finally as an intrinsic form of angular momentum carried by elementary particles. State-of-the-art laser technology has been expected to stimulate the experimental investigation of laser-matter interactions in the ultrarelativistic regime [3–5] where spin effects can set in. In the theoretical aspect, spin effects have been shown to participate in relativistic laser-electron interactions [6,7], in relativistic laser-atom interactions [8,9], in an electron's Kapitza-Dirac scattering from a standing laser wave [10,11], in production of electron-positron pairs [12,13], and so on.

Free-electron dynamics in high-intensity laser fields are of fundamental importance and have encountered sustained interest in many fields of physics [14,15]. With the present laser intensity beyond $10^{22}\,\mathrm{W/cm^2}$ [16], the commonly used description of electrons as spinless particles is put into doubt because an electron can couple to an external electromagnetic field via its charge as well as via its spin [17]. In this regard, a particular question is to what extent the spin degree of freedom of an electron may influence its orbital dynamics.

Spin is an essential part of the Dirac equation [18] in relativistic quantum mechanics, implied by the four-component spinor wave function. Theoretically, the Dirac equation describes all the dynamical information of a spin-1/2 massive particle. It is, however, not very transparent for physical interpretation. Besides the quantum spin theory, classical spin theories were developed independently. In 1926, Frenkel [19] established the first classical theory of a charged particle with an intrinsic magnetic moment representing its spin. Commenced with Frenkel's pioneering work, Weyssenhoff and Raabe [20], Nagy [21], Bhabha and Corben [22], etc. were also devoted to the classical equations of motion of a spinning particle, see the review articles of Nyborg [23] and Bagrov and Bordovitsyn [24]. Not long ago, semiclassical equations of motion of orbital and spin were deduced by Silenko [25] from a classical limit of the Foldy-Wouthyusen transformation of the Dirac equation. Classical theories can reveal the interaction of spin and orbital explicitly. They are usually easier to interpret than the quantum theory.

In the year of 1999, Walser *et al.* [17] began to study the electron dynamics with spin in a classical framework by using a relativistic equation of motion including the spin-laser interaction. They realized that the electron's motion from rest in a linearly polarized plane-wave laser field can become three-dimensional depending on the initial spin, owing to the spin-induced force in the magnetic-field direction. Then they confirmed the classical results by a quantum-mechanically analytical calculation in the weakly relativistic limit [26]. Later, Roman *et al.* [27] gave the first exact evidence of the spin-induced force according to the exact three-dimensional solutions of the Dirac equation describing an electron driven by a linearly polarized plane-wave laser field [28].

Realistic laser pulses produced in laboratories may have more complicated structures than plane waves. In this paper, we promote the investigation of electron dynamics with spin in linearly polarized standing-wave fields where there are no exact solutions of the Dirac equation. Our calculations rely on numerically solving the three-dimensional Dirac equation which is applicable to arbitrary laser fields. The remaining parts of this paper are arranged as follows. In Sec. II, we introduce the theoretical foundations of our studies, including the Dirac equation and a classical spin model. Results and discussions are presented in Sec. III, where we calculated the spin-dependent dynamics of quantum wave packets and

*fuyongsheng@nudt.edu.cn
†jlzeng@nudt.edu.cn
‡jmyuan@nudt.edu.cn

classical electrons in both plane-wave and standing-wave fields. Lastly, Sec. IV gives the conclusion. Atomic units with the electron charge and mass satisfying $-e = m_e = 1$ are used throughout the paper.

II. THEORETICAL FOUNDATIONS

In this section, the quantum and classical descriptions of a spinning particle interacting with an external electromagnetic field are introduced. Radiation reaction [29] is not included here.

A. Dirac equation

The relativistic quantum dynamics of a spin-1/2 particle of the rest mass m and charge q in an external electromagnetic field characterized by the potentials $\boldsymbol{A}(\boldsymbol{r},t)$ and $\phi(\boldsymbol{r},t)$ is governed by the time-dependent Dirac equation [30,31],

$$i\dot{\Psi}(\boldsymbol{r},t) = \{c\boldsymbol{\alpha}\cdot[-i\boldsymbol{\nabla} - q\boldsymbol{A}(\boldsymbol{r},t)/c] + mc^2\beta + q\phi(\boldsymbol{r},t)\}\Psi(\boldsymbol{r},t), \tag{1}$$

where $\Psi(\boldsymbol{r},t)$ is the four-component wave function at the space-time $\boldsymbol{r} = (x,y,z)^T$ and t, $\boldsymbol{\alpha}$, β denote the Dirac matrices written explicitly as

$$\boldsymbol{\alpha} = \begin{pmatrix} 0 & \boldsymbol{\sigma} \\ \boldsymbol{\sigma} & 0 \end{pmatrix},\ \beta = \begin{pmatrix} I & 0 \\ 0 & -I \end{pmatrix}, \tag{2}$$

with $\boldsymbol{\sigma} = (\sigma_x,\sigma_y,\sigma_z)^T$ the Pauli matrices and I the unit matrix of 2×2.

The positive-energy solutions of Eq. (1) with vanishing $\boldsymbol{A}$ and ϕ are

$$\Psi_{\boldsymbol{p},s} = \sqrt{\frac{E_{\boldsymbol{p}}+mc^2}{2VE_{\boldsymbol{p}}}}\begin{pmatrix} \chi_s \\ \frac{c\boldsymbol{\sigma}\cdot\boldsymbol{p}}{E_{\boldsymbol{p}}+mc^2}\chi_s \end{pmatrix}\exp(-ip_\mu x^\mu), \tag{3}$$

where χ_s is the two-component spinor, $E_{\boldsymbol{p}} = \sqrt{\boldsymbol{p}^2c^2+m^2c^4}$ denotes the relativistic energy, $p_\mu = (E_{\boldsymbol{p}}/c, -\boldsymbol{p})^T$ and $x^\mu = (ct,\boldsymbol{r})^T$ are the four vectors of momentum and position, V is a normalization volume.

Either wave function of Eq. (3) has a definite momentum but distributes throughout space. The plane-wave form fails to describe a propagating particle which is always localized in space. For this, we use wave packets. They are superpositions of plane waves which yield localized wave functions. Especially, we define the Gaussian wave packet as

$$\Psi_{G,s} = \mathcal{N}\int \exp\left(-\frac{\boldsymbol{p}^2}{\delta^2}\right)\Psi_{\boldsymbol{p},s}d^3p, \tag{4}$$

where $\mathcal{N}$ is the normalization constant, δ is width of the Gaussian distribution in momentum space. The wave packet (4) is constructed by superimposing the positive-energy solutions (3) at all momentums $\boldsymbol{p}$ weighted by a Gaussian distribution. It represents a Dirac particle at rest centered at the origin $\boldsymbol{r} = \boldsymbol{0}$ at the time $t = 0$. Notice that there are no negative-energy components in the resulting wave function $\Psi_{G,s}$, different from those in Refs. [28,32].

The wave packet (4) has a definite spin decided entirely by χ_s. We choose

$$\chi_s = \frac{1}{\sqrt{2}}\begin{pmatrix}1\\1\end{pmatrix},\quad \chi_s = \frac{1}{\sqrt{2}}\begin{pmatrix}1\\i\end{pmatrix},\quad \text{and}\quad \chi_s = \begin{pmatrix}1\\0\end{pmatrix}, \tag{5}$$

which are the eigenvectors of the Pauli matrices σ_x, σ_y, and σ_z for the spins in the x, y, and z directions, respectively.

The quantum dynamics is obtained by solving the Dirac equation numerically, from the constructed Gaussian wave packet. We utilize the Fourier split-operator method [33,34]. The basic idea is to replace the time-evolution operator by a product of operators that are diagonal either in real space or in momentum space and to propagate the wave function alternately in real space and momentum space. The wave function is discretized on a three-dimensional self-adaptive Cartesian grid and distributed among computer processors using a domain-decomposition strategy. On this basis, the transform of the wave functions between both spaces is implemented by a parallel fast-Fourier-transform algorithm.

B. Classical spin model

Here we obtain the equations of motion of a classical particle with spin in an electromagnetic field from the Lagrangian formalism [17,35]. Considering spin-field interaction, the Lagrangian of the particle with the mass m and charge q is written as

$$\mathcal{L} = \frac{mc^2}{\gamma} + \frac{q}{c\gamma}A_\alpha u^\alpha + \frac{1}{2\gamma}\mu^{\alpha\beta}F_{\alpha\beta}, \tag{6}$$

where $\gamma = (1-\boldsymbol{v}^2/c^2)^{-1/2}$ is the relativistic Lorentz factor, $u^\alpha = \gamma(c,\boldsymbol{v})$ is the four velocity, $A^\alpha = (\phi,\boldsymbol{A})$ is the four-potential of the electromagnetic field, $\mu^{\alpha\beta}$ is the antisymmetric Frenkel tensor,

$$\mu^{\alpha\beta} = \begin{pmatrix} 0 & -d_x & -d_y & -d_z \\ d_x & 0 & m_z & -m_y \\ d_y & -m_z & 0 & m_x \\ d_z & m_y & -m_x & 0 \end{pmatrix}, \tag{7}$$

defined in terms of the particle's magnetic moment $\boldsymbol{m} = (m_x,m_y,m_z)^T$ and electric dipole moment $\boldsymbol{d} = (d_x,d_y,d_z)^T$ in the laboratory frame, $F^{\alpha\beta}$ is the electromagnetic field tensor

$$F_{\alpha\beta} = \begin{pmatrix} 0 & E_x & E_y & E_z \\ -E_x & 0 & -B_z & B_y \\ -E_y & B_z & 0 & -B_x \\ -E_z & -B_y & B_x & 0 \end{pmatrix} \tag{8}$$

made from the electric field $\boldsymbol{E} = (E_x,E_y,E_z)^T$ and magnetic field $\boldsymbol{B} = (B_x,B_y,B_z)^T$. In the above expressions, we take the metric $g^{\alpha\beta} = \mathrm{diag}(1,-1,-1,-1)$.

The Lagrangian (6) can be rewritten in a three-dimensional form as

$$\mathcal{L} = \frac{mc^2}{\gamma} - \frac{q}{c}\boldsymbol{A}\cdot\boldsymbol{v} + q\phi - \frac{\chi}{\gamma}(\boldsymbol{\zeta}\cdot\boldsymbol{B} + \boldsymbol{\tau}\cdot\boldsymbol{E}), \tag{9}$$

where we introduce the dimensionless moments $\boldsymbol{\zeta}$ and $\boldsymbol{\tau}$, satisfying $\boldsymbol{m} = \chi\boldsymbol{\zeta}$ and $\boldsymbol{d} = \chi\boldsymbol{\tau}$. χ is defined so $\boldsymbol{\zeta}$ equals to the spin vector $\boldsymbol{s}$ when the particle is at rest. Hence $\chi = g_s q/2mc$, where g_s is the dimensionless quantity called the spin g-factor.

In the present paper, we use $g_s = 2$ exactly for the electron, ignoring the intrinsic anomalous magnetic moment.

Substituting Eq. (9) into the Euler-Lagrange equation,

$$\frac{d}{dt}\left(\frac{\partial \mathcal{L}}{\partial \boldsymbol{v}}\right) = \frac{\partial \mathcal{L}}{\partial \boldsymbol{r}}, \tag{10}$$

and making use of the relationship between the field and potential,

$$\boldsymbol{E} = -\frac{1}{c}\frac{\partial \boldsymbol{A}}{\partial t} - \nabla\phi, \quad \boldsymbol{B} = \nabla \times \boldsymbol{A}, \tag{11}$$

we obtain the equation of motion of the momentum,

$$M\frac{d(\gamma \boldsymbol{v})}{dt} = \boldsymbol{F}_0 + \boldsymbol{F}_s, \tag{12}$$

where

$$M = m - \frac{\chi}{c^2}(\boldsymbol{\zeta}\cdot\boldsymbol{B} + \boldsymbol{\tau}\cdot\boldsymbol{E}) \tag{13}$$

represents the effective mass due to spin-field interaction,

$$\boldsymbol{F}_0 = q\boldsymbol{E} + \frac{q}{c}\boldsymbol{v}\times\boldsymbol{B} \tag{14}$$

is the lorentz force of charge, and

$$\begin{aligned}\boldsymbol{F}_s = {} & \frac{\chi}{\gamma}\nabla(\boldsymbol{\zeta}\cdot\boldsymbol{B} + \boldsymbol{\tau}\cdot\boldsymbol{E}) + \frac{\gamma\chi}{c^2}\boldsymbol{v}\frac{d}{dt}(\boldsymbol{\zeta}\cdot\boldsymbol{B} + \boldsymbol{\tau}\cdot\boldsymbol{E}) \\ & - \frac{\chi}{c\gamma}\frac{d}{dt}(\boldsymbol{\zeta}\times\boldsymbol{E}) + \frac{\gamma\chi}{c^3}\boldsymbol{v}\cdot\frac{d\boldsymbol{v}}{dt}(\boldsymbol{\zeta}\times\boldsymbol{E})\end{aligned} \tag{15}$$

is the additional spin-induced force. We can see Eq. (12) reduces to the well-known Lorentz equation for a spinless particle when $\mu^{\alpha\beta} = 0$.

The spin-induced force $\boldsymbol{F}_s$ has a dependence on the time derivatives of the moments which are determined by the equation of motion of the Frenkel tensor $\mu^{\alpha\beta}$,

$$\frac{1}{\chi}\frac{d\mu^{\alpha\beta}}{ds} = F^{\alpha}_{\ \rho}\mu^{\rho\beta} - F^{\beta}_{\ \rho}\mu^{\rho\alpha}, \tag{16}$$

or equivalently by the equations of motion of the moments

$$\frac{d\boldsymbol{\zeta}}{dt} = \frac{\chi}{\gamma}(\boldsymbol{\zeta}\times\boldsymbol{B} + \boldsymbol{\tau}\times\boldsymbol{E}), \tag{17}$$

$$\frac{d\boldsymbol{\tau}}{dt} = \frac{\chi}{\gamma}(-\boldsymbol{\zeta}\times\boldsymbol{E} + \boldsymbol{\tau}\times\boldsymbol{B}). \tag{18}$$

Besides, $\boldsymbol{F}_s$ also has a dependence on the gradients of the electromagnetic fields. Here the time derivatives of the fields must be interpreted as the convective derivative $d/dt = \partial/\partial t + \boldsymbol{v}\cdot\nabla$.

Up to now, the Eq. (12) we obtained is exact. It is, however, in an implicit form with the acceleration-dependent term in $\boldsymbol{F}_s$. We use the same resolvent as Ref. [17], making the approximation

$$\boldsymbol{v}\cdot\frac{d\boldsymbol{v}}{dt} \approx \frac{q}{m}\frac{\boldsymbol{v}\cdot\boldsymbol{E}}{\gamma^3}, \tag{19}$$

according to the Lorentz equation. As a result, Eq. (12) with Eqs. (17), (18), and the equation of motion of position

$$\frac{d\boldsymbol{r}}{dt} = \boldsymbol{v} \tag{20}$$

makes up a system of differential equations obeying an initial value problem which allows a direct numerical integration.

III. RESULTS AND DISCUSSIONS

In the present paper, we investigate the spin-dependent dynamics of electrons in linearly polarized standing-wave fields. We use the laser pulse with a smooth turn-on and turn-off, the electric field of which reads

$$\boldsymbol{E}(\boldsymbol{r}, t) = \boldsymbol{e}_y E_0 \cos(kx) F(\omega t)\cos(\omega t), \tag{21}$$

where $\boldsymbol{e}_y$ is the polarization vector in the y direction, E_0 is the peak electric-field amplitude, ω is the angular frequency, $k = \omega/c$ is the modulus of the wave vector in the x direction, $F(\theta)$ is a $\sin^2$-shaped envelope function,

$$F(\theta) = \begin{cases} \sin^2\left(\frac{\theta}{8}\right), & 0 \leqslant \theta < 4\pi \\ 1, & 4\pi \leqslant \theta < (2N+4)\pi \\ \sin^2\left(\frac{(2N+8)\pi-\theta}{8}\right), & (2N+4)\pi \leqslant \theta \leqslant (2N+8)\pi, \end{cases} \tag{22}$$

with two-cycle turn-on phase, N-cycle constant phase, and two-cycle turn-off phase. The electric field (21) has nodes and antinodes at the locations $(2l+1)\lambda/4$ and $l\lambda/2$, where l is an integer and $\lambda = 2\pi/k$ is the laser wavelength. The corresponding vector potential reads

$$\boldsymbol{A}(\boldsymbol{r}, t) = -\boldsymbol{e}_y\frac{cE_0}{\omega}\cos(kx)\int_0^{\theta} F(\theta')\cos(\theta')d\theta', \tag{23}$$

where $\theta = \omega t$. The magnetic-field is obtained by $\boldsymbol{B} = \nabla\times\boldsymbol{A}$,

$$\boldsymbol{B}(\boldsymbol{r}, t) = \boldsymbol{e}_z E_0 \sin(kx)\int_0^{\theta} F(\theta')\cos(\theta')d\theta', \tag{24}$$

having nodes and antinodes contrary to the electric field.

Calculations are carried out by numerically solving the time-dependent Dirac Eq. (1) from Gaussian wave packets (4) and integrating the coupled differential Eqs. (12), (17), (18), and (20) of classical electrons using the Runge-Kutta algorithm.

A. Plane-wave fields

Before the main work, it is of benefit to give a confirmation of the known results for linearly polarized plane-wave laser fields. We use the laser pulse whose electric field reads

$$\boldsymbol{E}(\boldsymbol{r}, t) = \boldsymbol{e}_y E_0 F(\eta)\cos(\eta), \tag{25}$$

where $F(\eta)$ is the envelope function (22) with $\eta = \omega t - kx$.

A localized quantum wave packet in a linearly polarized plane-wave field undergoes an oscillation in the laser polarization direction and a drift in the laser propagation direction, with its spreading and shearing. This can be seen from the existing two-dimensional implementations in solving the Dirac equations so far [33,36,37].

For our three-dimensional solutions, visualization of the wave packet uses the two-dimensional probability densities, which are obtained by integrating the probability densities in the direction perpendicular to the polarization-propagation plane $\rho = \int |\Psi|^2 dz$. In the calculations, we use the Gaussian wave packet with the momentum width $\delta = 2$ a.u. and spin

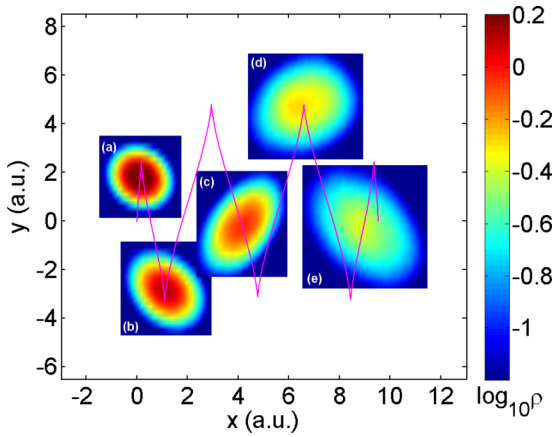

FIG. 1. Wave-packet evolution in the linearly polarized plane-wave field as shown by the logarithm of the two-dimensional probability densities $\rho = \int |\Psi|^2 dz$ at the times (a) 0.25 a.u., (b) 0.5 a.u., (c) 0.75 a.u., (d) 1 a.u., (e) 1.25 a.u.. Also shown by the magenta (grey) solid line is the two-dimensional components $(\bar{x}(t), \bar{y}(t))$ of the center-of-mass trajectory $\bar{\boldsymbol{r}}(t) = \int |\Psi|^2 \boldsymbol{r} dx dy dz$. Calculations are made for the Gaussian wave packet (4) of momentum width 2 a.u. (the same below) and spin in the x direction in the plane-wave field (25) of electric-field amplitude $E_0 = 1600$ a.u., angular frequency $\omega = 20$ a.u., and five cycles ($N = 1$).

in the x direction, as well as the laser field of electric-field amplitude $E_0 = 1600$ a.u., angular frequency $\omega = 20$ a.u., and five cycles ($N = 1$). Figure 1 gives the wave-packet evolution, along with the two-dimensional components $(\bar{x}(t), \bar{y}(t))$ of the center-of-mass trajectory $\bar{\boldsymbol{r}}(t) = \int |\Psi|^2 \boldsymbol{r} dx dy dz$. At this time, Fig. 1 is not significantly different from the two-dimensional results.

However, Fig. 1 hides the possible three-dimensional motion caused by spin. We understand this when we plot all three components of $\bar{\boldsymbol{r}}(t)$. As shown in Fig. 2, we compare the center-of-mass trajectories of the quantum wave packets and the trajectories of the classical electrons, with Figs. 2(a), 2(b) and 2(c) corresponding to the initial spins in the *x, y,* and z directions, respectively. The electron dynamics are shown to have a high dependence on the initial spin. Specifically, the electrons undergo three-dimensional motions moving out of the polarization-propagation plane when their spins are initially perpendicular to the magnetic field, as seen in the top two panels, otherwise the electron always stays in the plane when its spin is initially parallel to the magnetic field, as seen in the bottom panel. The quantum and classical results are in good agreement.

Figure 2 evidently reveals the differences in the z components of the trajectories. In fact, the spin also modifies the ordinary Lorentz dynamics in the x and y directions. Nevertheless, because the amplitudes of the spin-induced forces are extremely small compared with the Lorentz force, there are no sharp differences in the two-dimensional components of the trajectories along the polarization-propagation plane.

We have obtained similar results as Roman *et al.* for the plane-wave field. On this basis, we turn to the standing-wave fields. Different field strengths and pulse lengths are taken into account.

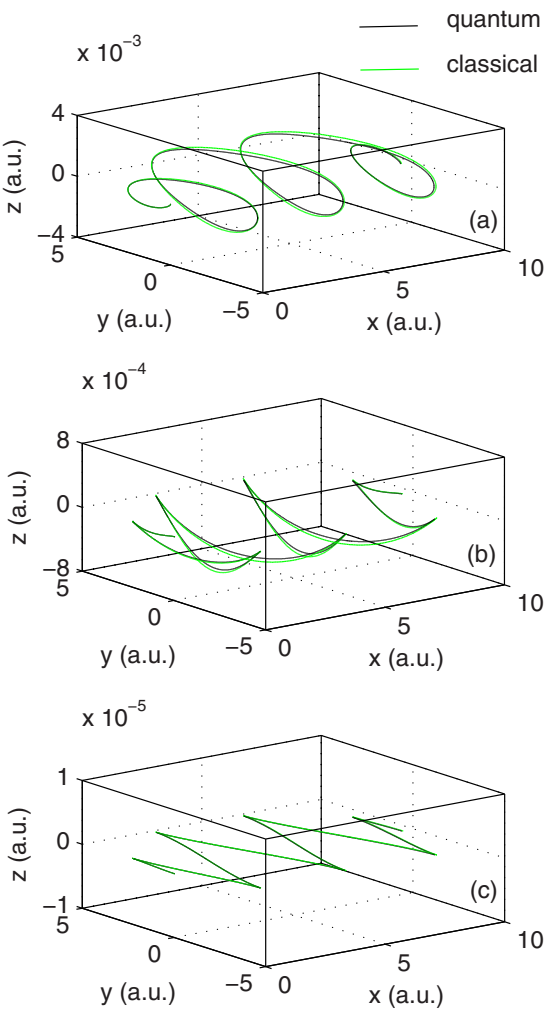

FIG. 2. Center-of-mass trajectories of the quantum wave packets as well as the trajectories of the classical electrons in the same plane-wave field as Fig. 1. The black and green (light grey) lines stand for the quantum and classical results. The three panels (a), (b), and (c) correspond to the initial spins in the *x, y,* and z directions.

B. Standing-wave fields

For the plane-wave field, the wave packet moves as a whole along its center of mass, as seen in Fig. 1. Things change when we turn to the standing-wave field. In Fig. 3, the evolution from the same Gaussian wave packet as Fig. 1 is calculated for the standing-wave field of the same E_0, ω, and number of cycles. We can see that the wave packet does not keep integrity all the time but spreads heavily along the polarization-propagation plane. The scenario can be understood classically by analyzing the forces exerting on the different parts. When the wave packet is prepared around the maximum of the electric field, it is driven by the electric-field force and moves vertically from rest. Due to the finite width of the wave packet, the left and right parts deviating from the center suffer the magnetic-field forces in opposite directions and travel laterally apart from each other. With the spreading, the wave packet experiences the spatial variation of the electric and magnetic fields both in amplitudes and directions. The evolution becomes complex with the different

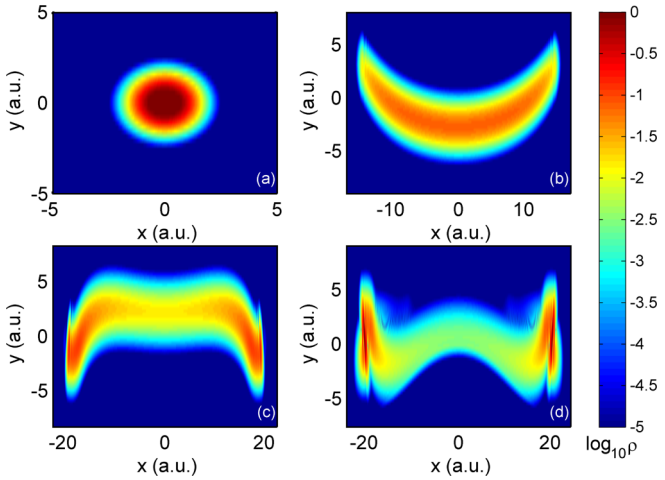

FIG. 3. Wave-packet evolution in the linearly polarized standing-wave field as shown by the logarithm of the two-dimensional probability densities $\rho = \int |\Psi|^2 dz$ at the times (a) 0 a.u., (b) 0.8 a.u., (c) 1 a.u., (d) 1.2 a.u.. Calculations are made for the Gaussian wave packet with the spin in the x direction in the standing-wave field (21) of peak electric-field amplitude $E_0 = 1600$ a.u., angular frequency $\omega = 20$ a.u., and five cycles ($N = 1$).

parts moving in different directions. There may be overlaps of them which result in many interference patters.

To add further evidence to the above classical analysis, we use a trick simulating the join trajectories of an ensemble of classical particles. The ensemble is made of 100 000 classical electrons, initially in the polarization-propagation plane of z = 0, whose coordinates and momentums obey the two-dimensional Gaussian distributions analogous to the space and momentum distributions of the Gaussian wave packet in the x and y directions. All the electrons are independent, obeying the equations of motion of a classical particle with spin. Figure 4 shows the two-dimensional projections of the classical ensemble on to the polarization-propagation plane at the same four times as the quantum evolution in Fig. 3. We can see that the probability densities of the quantum wave packet and the electron distributions of the classical ensemble match very well except for the quantum interference.

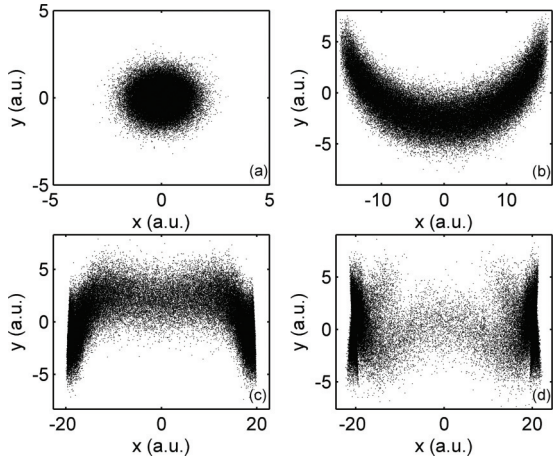

FIG. 4. Evolution of an ensemble of 100 000 classical electrons, which simulates the evolution of the quantum wave packet in Fig. 3.

As before, the above two-dimensional plots hide the possible three-dimensional motions caused by spin. Different from the plane-wave field for which the spin-dependent features are well manifested in the centroid dynamics, the spin-dependent dynamics for the standing-wave field should be distinguished for the different parts of the wave packet along the polarization-propagation plane. For this purpose, we define the local displacement of the wave packet in the z direction at any point (x, y) as

$$D_z = \frac{\int |\Psi|^2 z dz}{\int |\Psi|^2 dz}. \tag{26}$$

In the following, D_z are calculated for the wave packets with different initial spins at the selected times of the evolutions. To support the results, the comparable quantities are calculated (see the Appendix) for the ensemble of classical electrons.

We have shown the results in Figs. 5 and 6, where the local displacements are indicated by the two-dimensional pseudocolor maps. Figure 5 corresponds to the initial spin in the x direction. Figure 6 corresponds to the initial spin in the y direction. As is shown, in both cases, there are spin-induced nonzero displacements varying from one point to another and changing with time, and the quantum wave packets are well simulated by the classical ensembles. In addition, the initial spin has a decisive influence on the distribution of

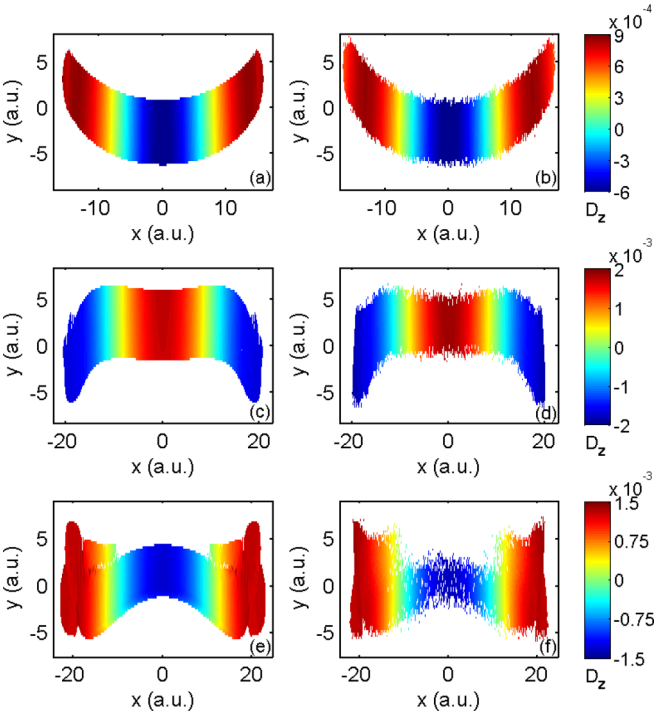

FIG. 5. Spin-induced local displacements in the z direction. (a), (c), (e) are the results of the quantum wave packet at the times 0.8 a.u., 1 a.u., 1.2 a.u. according to Eq. (26) and display only the points where $\rho = \int |\Psi|^2 dz > 10^{-5}$ a.u. (b), (d), (f) are the results of the classical ensemble at the corresponding times according to Eq. (A2). Calculations are made for the quantum wave packet and classical ensemble with the initial spin in the x direction in the standing-wave field of peak electric-field amplitude $E_0 = 1600$ a.u., angular frequency $\omega = 20$ a.u., and five cycles ($N = 1$).

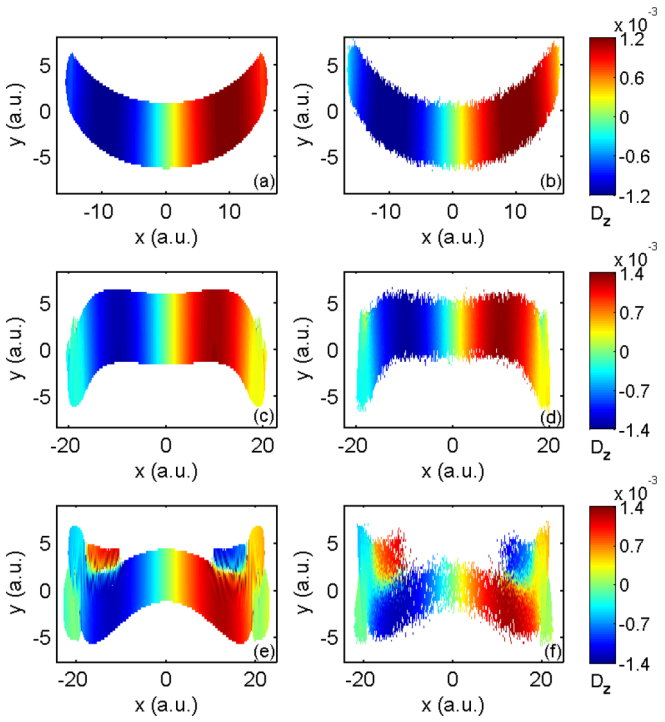

FIG. 6. The same as Fig. 5 but for the initial spin in the y direction.

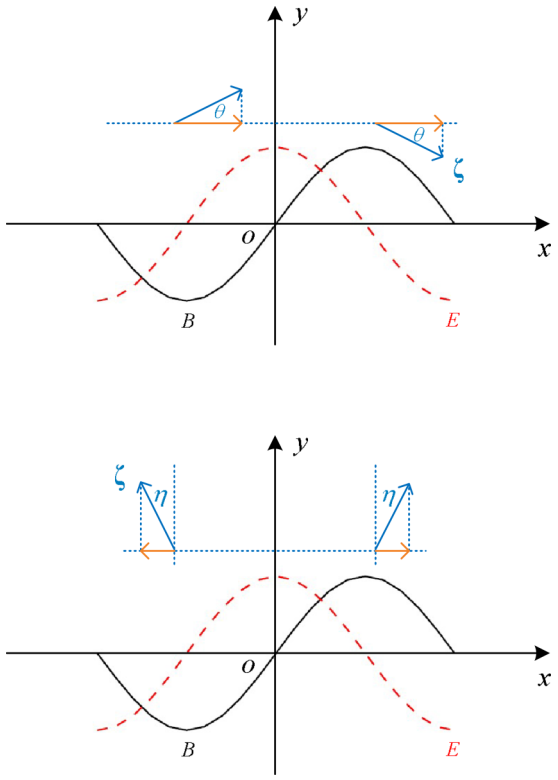

FIG. 7. Precessions of the moments $\boldsymbol{\zeta}$ for the initial spins in the x direction (top) and y direction (bottom). The black solid lines and the red dashed lines stand for a sketch of the instant magnetic and electric fields. θ and η are the angles of the precessing moments relative to the initial directions. For each initial spin, we make a comparison of the product $\boldsymbol{\zeta} \times \boldsymbol{E}$ at the symmetric positions about the plane $x = 0$. Considering the polarization, only the projections in the x direction take effect.

the local displacements at a moment, leading to symmetric distributions about the plane $x = 0$ in Fig. 5 but antisymmetric distributions in Fig. 6. Notice that we have omitted the case of the initial spin in the z direction, because the motion is confined in the polarization-propagation plane.

The symmetry of the displacements can be explained classically by analyzing the symmetry of the spin-induced forces. When the initial spin is perpendicular to the magnetic field, as in either case, the first two terms of Eq. (15) vanish, the spin-induced force being an odd function of the product $\boldsymbol{\zeta} \times \boldsymbol{E}$. We need to compare the products at the symmetric positions about the plane $x = 0$. This is done in Fig. 7 by following the precessions of the moments $\boldsymbol{\zeta}$ around the magnetic field. Due to the asymmetry of the magnetic field about $x = 0$, the moments at the symmetric positions must precess in the opposite directions. For the initial spin in the x direction, the products are equal, resulting in a symmetric distribution of the spin-induced forces. But for the initial spin in the y direction, the products are equal and opposite resulting in an asymmetric distribution.

The above results are obtained for the standing-wave field of a low field strength and short pulse. In the following, the spin-dependent dynamics are examined for the field of a high field strength and long pulse. We increase the peak electric-field amplitude to $E_0 = \omega c$, leaving the angular frequency unchanged at $\omega = 20$ a.u. This indicates that even if an electron is initially at rest, it becomes relativistic within almost one laser period. Considering a ten-cycle pulse having a six-cycle constant phase, in Figs. 8 and 9, the spin-induced local displacements are compared between the quantum theory and the classical spin model in the same way as Figs. 5 and 6. We can see that the quantum wave packets are well simulated by the classical ensembles, also at the high field strength and long pulse. However, there are more interference patterns in the quantum results coming from more overlaps of different parts of the wave packets during the long-time evolution. At last, the symmetries of both figures meet our earlier analysis.

We have confirmed the spin-dependent dynamics of quantum wave packets in linearly polarized standing-wave fields. There are indeed net three-dimensional motions when the initial spins are perpendicular to the magnetic field, owned by the different parts of the wave packets along the polarization-propagation plane. However, there are no sharp differences in the evolutions of the wave packets with different initial spins as seen from the two-dimensional probability densities.

The dynamics of a classic particle in a standing-wave field become chaotic above a certain field strength, where a slight change in the initial condition produces a totally different trajectory [38]. In the next stage, we observe the electron spin-dependent dynamics in the chaotic regime, focusing only on the two-dimensional motions along the polarization-propagation plane. We use the peak electric-field amplitude $E_0 = \omega c$ lying above the critical field strength and the 100-cycles pulse ($N = 96$) long enough to cover the chaotic motion.

At first, the trajectories are calculated for the classical electrons of different initial spins, from the same initial position

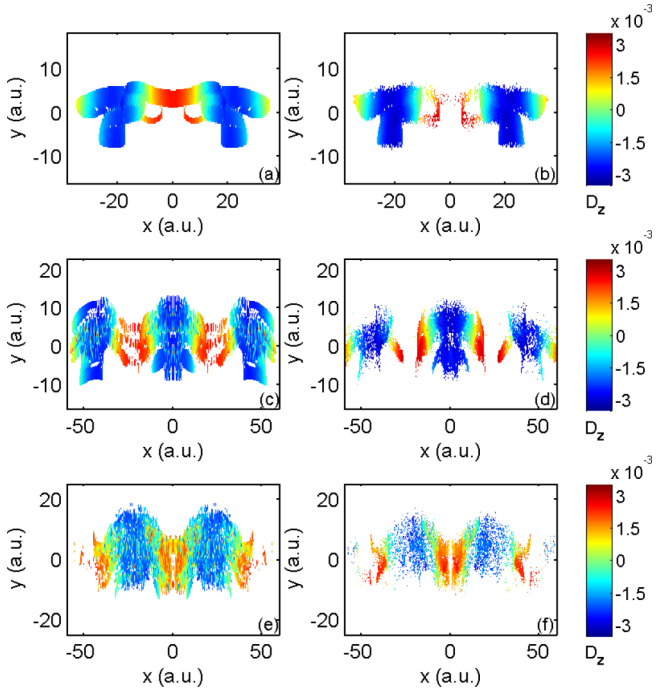

FIG. 8. Spin-induced local displacements in the z direction. (a), (c), (e) are the results of the quantum wave packet at the times 1 a.u., 1.5 a.u., 2 a.u. according to Eq. (26) and display only the points where $\rho = \int |\Psi|^2 dz > 10^{-4}$ a.u.. (b), (d), (f) are the results of the classical ensemble at the corresponding times according to Eq. (A2). Calculations are made for the quantum wave packet and classical ensemble with the initial spin in the x direction in the standing-wave field of peak electric-field amplitude $E_0 = \omega c$, angular frequency $\omega = 20$ a.u., and ten cycles ($N = 6$).

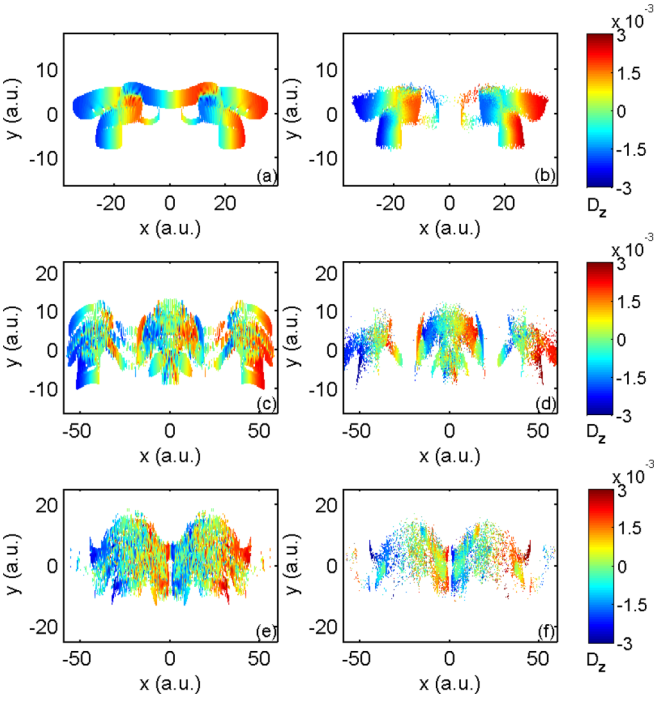

FIG. 9. The same as Fig. 8 but for the initial spin in the y direction.

and momentum. We show the results in Fig. 10. It can be seen that the electron trajectories vary differently with spin. This is because the small differences in the spin-induced forces finally cause significant differences in the trajectories, which is a clear signature of chaos. At this point, our calculations serve as proof of the occurrence of chaos. In the figure, we also see that the electron trajectories traverse many nodes of the field and have attractors around some nodes of the electric field.

Then a question is induced: What's the quantum correspondence to the classical chaotic dynamics? To answer the question, we need to solve the quantum dynamics for the same standing-wave field. We have verified the effectiveness of simulating the quantum wave-packet dynamics by the classical ensemble at the chaotic field strength for a short pulse. We expect that the long-time probability distribution of the quantum wave-packet would also be similar to the particle distribution of the corresponding classical ensemble. In view of this, we resort to pure classical calculations which make up the inefficiency in solving the Dirac equation for long-time evolutions. The results are summarized in Fig. 11. Among the three panels, the electrons in the ensembles have one-to-one the same initial positions and momentums but different initial spins. We can see that, though the trajectories vary differently with spin for individual electrons according to Fig. 10, there are no sharp differences in the whole particle distributions of the three ensembles. Especially, there are regular accumulations of the particles at the positions where the attractors of the classical trajectories lie. It could be expected that the quantum wave-packet dynamics in a classical chaotic regime would display a space-time probability distribution

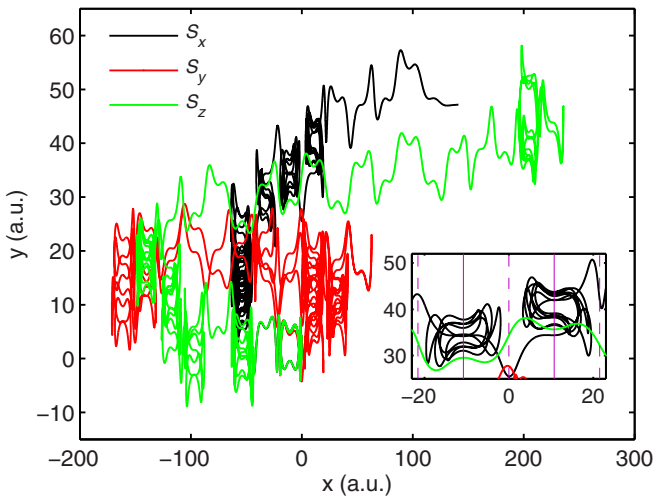

FIG. 10. Two-dimensional components of the trajectories of the classical electrons along the polarization-propagation plane. The black, red (medium grey), and green (light grey) lines stand for the initial spins in the x, y, and z directions, respectively. Calculations are made for the electrons with the same initial position $\boldsymbol{r}_0 = (0.3, -0.3, 0)$ a.u. and momentum $\boldsymbol{p}_0 = (-2.0, 1.7, 0)$ a.u. but different initial spins in the standing-wave field of peak electric-field amplitude $E_0 = \omega c$, angular frequency $\omega = 20$ a.u., and 100 cycles ($N = 96$). The inset gives an enlarged view of the selected range where the vertical solid and dashed lines stand for the nodes and antinodes of the electric field.

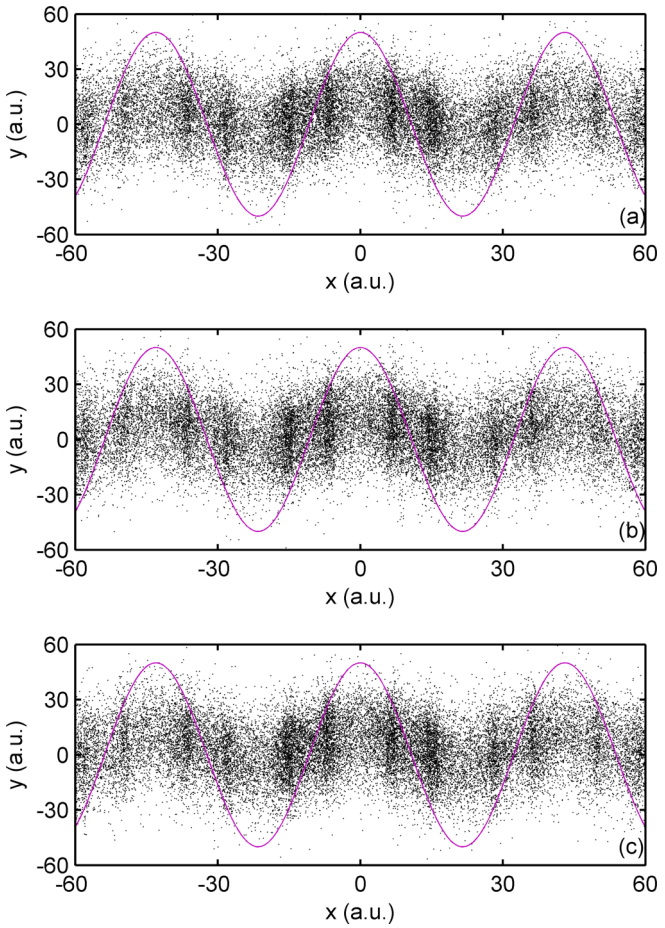

FIG. 11. Evolutions of the three ensembles of classical electrons with one-to-one the same initial positions and momentums but different initial spins in the same standing-wave field as Fig. 10 at the selected time $t = 11$ a.u. The three panels (a), (b), and (c) correspond to the initial spins in the x, y, and z directions. The magenta (grey) solid line in each panel stands for the electric field (with arbitrary units) at this time.

with apparent features of classical attractor distributions. From the quantum mechanical point of view, the regular distribution of the space-time probability densities corresponds to the distribution of the structured momentums and energy spectra, which was observed in the quantum dynamics of the corresponding classical chaotic systems [39–41]. Lastly, we need to say that the reasoning on the quantum results need to be proved by solving the Dirac equation for the long pulse. Actually, more studies are needed to find the whole quantum nature of a classical chaotic system, including how the quantum coherence works in the classical chaotic regime.

IV. CONCLUSION

The present paper is devoted to relativistic electron motions in linearly polarized laser fields, with a particular attention to the spin effects. The spin-dependent dynamics are identified for the quantum wave packets by numerically solving the three-dimensional Dirac equation and for the classical electrons by using a classical spin model.

We give confirmation of the known results for plane-wave fields that an electron initially at rest can experience a three-dimensional motion moving out the polarization-propagation plane due to spin. The center of mass of a quantum wave packet behaves like a classical electron.

We study the wave-packet evolutions in the standing-wave fields of different strengths and pulse lengths. The wave packets spread heavily along the polarization-propagation plane when they are initially put at an antinode of the electric field. There may be net motions in the magnetic-field direction for different parts of the wave packets. The quantum dynamics have no classical counterparts in the single-particle sense, but are well simulated by the ensembles of classical electrons.

In the chaotic regime of a standing-wave field, the classical single particle dynamics are very sensitive to the initial spins and show many attractors in the trajectories. However, the classical ensemble dynamics with different initial spins results in approximately a definite particle distribution in space and time which reflects the most essential features of the classical chaotic dynamics, i.e., the distribution of attractors in space and time.

ACKNOWLEDGMENTS

This work was supported by Science Challenge Project No. TZ2018005, by the National Key R&D Program of China under Grant No. 2017YFA0403202, and by the National Natural Science Foundation of China under Grants No. 11674394 and No. 11774322. The work was carried out at National Supercomputer Center in Tianjin, and the calculations were performed on TianHe-1(A).

APPENDIX

We report here the manner of calculating the comparable quantity of Eq. (26) from the ensemble of classical particles. It is based on the Cartesian-grid-based method [34] in numerically solving the Dirac equation.

Suppose the computational rectangular area along the polarization-propagation (xy) plane is discretized as

$$\begin{aligned} x_i &= x_{\min} + (i-1)\Delta x, \quad i = 1, \cdots, \quad n_x, \\ y_j &= y_{\min} + (j-1)\Delta y, \quad j = 1, \cdots, \quad n_y, \end{aligned} \tag{A1}$$

where $x_{\min}$, $y_{\min}$ are the lower bounds of the area, n_x, n_y are the numbers of the grid points in the x and y directions, Δx, Δy are the grid steps.

With this, the particles in the ensemble are tied to the specific grid point (x_i, y_j) if their x and y coordinates lie in the interval $[x_i - \Delta x/2, x_i + \Delta x/2] \times [y_j - \Delta y/2, y_j + \Delta y/2]$, and meanwhile the number of them is counted as N_{ij}. Thus we have $\sum_{ij} N_{ij} = N$, where N is the total number of the particles in the ensemble.

Lastly, the local displacement of the ensemble at the point (x_i, y_j) in the z direction is calculated by averaging the z coordinates of the particles around the point (x_i, y_j) as

$$D_z = \frac{1}{N_{ij}} \sum_{k=1}^{N_{ij}} z_k. \tag{A2}$$

[1] G. E. Uhlenbeck and S. Goudsmit, Spinning electrons and the structure of spectra, Nature (London) **117**, 264 (1926).

[2] W. Gerlach and O. Stern, Der experimentelle nachweis der richtungsquantelung im magnetfeld, Z. Phys. **9**, 349 (1922).

[3] Y. I. Salamin, S. X. Hu, K. Z. Hatsagortsyan, and C. H. Keitel, Relativistic high-power laser-matter interactions, Phys. Rep. **427**, 41 (2006).

[4] F. Ehlotzky, K. Krajewska, and J. Z. Kamiński, Fundamental processes of quantum electrodynamics in laser fields of relativistic power, Rep. Prog. Phys. **72**, 046401 (2009).

[5] A. Di Piazza, C. Müller, K. Z. Hatsagortsyan, and C. H. Keitel, Extremely high-intensity laser interactions with fundamental quantum systems, Rev. Mod. Phys. **84**, 1177 (2012).

[6] H. Bauke, S. Ahrens, C. H. Keitel, and R. Grobe, Electron-spin dynamics induced by photon spins, New J. Phys. **16**, 103028 (2014).

[7] H. Bauke, S. Ahrens, and R. Grobe, Electron-spin dynamics in elliptically polarized light waves, Phys. Rev. A **90**, 052101 (2014).

[8] M. Klaiber, E. Yakaboylu, C. Müller, H. Bauke, G. G. Paulus, and K. Z. Hatsagortsyan, Spin dynamics in relativistic ionization with highly charged ions in super-strong laser fields, J. Phys. B **47**, 065603 (2014).

[9] E. Yakaboylu, M. Klaiber, and K. Z. Hatsagortsyan, Above-threshold ionization with highly charged ions in superstrong laser fields. III. Spin effects and their dependence on laser polarization, Phys. Rev. A **91**, 063407 (2015).

[10] R. Erhard and H. Bauke, Spin effects in Kapitza-Dirac scattering at light with elliptical polarization, Phys. Rev. A **92**, 042123 (2015).

[11] M. M. Dellweg and C. Müller, Controlling electron spin dynamics in bichromatic Kapitza-Dirac scattering by the laser field polarization, Phys. Rev. A **95**, 042124 (2017).

[12] T. O. Müller and C. Müller, Longitudinal spin polarization in multiphoton Bethe-Heitler pair production, Phys. Rev. A **86**, 022109 (2012).

[13] A. Wöllert, H. Bauke, and C. H. Keitel, Spin polarized electron-positron pair production via elliptical polarized laser fields, Phys. Rev. D **91**, 125026 (2015).

[14] A. K. Li, J. X. Wang, N. Ren, W. J. Zhu, X. Y. Li, R. Hoehn, and S. Kais, Harmonic generation from free electrons in intense laser fields: Classical versus semi-classical theory, Laser Phys. **24**, 015302 (2014).

[15] Y. I. Salamin and N. M. Jisrawi, Electron laser acceleration in vacuum by a quadratically chirped laser pulse, J. Phys. B **47**, 025601 (2014).

[16] V. Yanovsky, V. Chvykov, G. Kalinchenko, P. Rousseau, T. Planchon, T. Matsuoka, A. Maksimchuk, J. Nees, G. Cheriaux, G. Mourou, and K. Krushelnick, Ultra-high intensity-300-TW laser at 0.1 Hz repetition rate, Opt. Express **16**, 2109 (2008).

[17] M. W. Walser, C. Szymanowski, and C. H. Keitel, Influence of spin-laser interaction on relativistic harmonic generation, Europhys. Lett. **48**, 533 (1999).

[18] P. A. M. Dirac, The quantum theory of the electron, Proc. R. Soc. London Ser. A **117**, 610 (1928).

[19] J. Frenkel, The electrodynamics of rotating electrons, Z. Phys. **37**, 243 (1926).

[20] J. Weyssenhoff and A. Raabe, (1) Relativistic dynamics of spin-fluids and spin-particles, Nature **157**, 766 (1946).

[21] K. Nagy, Relativistic equation of motion for spinning particles, Acta Phys. Hung. **7**, 325 (1957).

[22] H. J. Bhabha and H. C. Corben, General classical theory of spinning particles in a Maxwell field, Proc. R. Soc. London A **178**, 273 (1941).

[23] P. Nyborg, On classical theories of spinning particles, Nuovo Cimento **23**, 47 (1962).

[24] V. G. Bagrov and V. A. Bordovitsyn, Classical spin theory, Sov. Phys. J. **23**, 128 (1980).

[25] A. J. Silenko, Foldy-Wouthyusen transformation and semiclassical limit for relativistic particles in strong external fields, Phys. Rev. A **77**, 012116 (2008).

[26] M. W. Walser and C. H. Keitel, Spin-induced force in intense laser-electron interaction, J. Phys. B **33**, L221 (2000).

[27] J. S. Roman, L. Roso, and L. Plaja, A complete description of the spin force, J. Phys. B **37**, 435 (2004).

[28] J. S. Roman, L. Plaja, and L. Roso, Relativistic quantum dynamics of a localized Dirac electron driven by an intense-laser-field pulse, Phys. Rev. A **64**, 063402 (2001)

[29] L. D. Landau and E. M. Lifshitz, *The Classical Theory of Fields* (Elsevier, Oxford, 1975).

[30] W. Greiner, *Relativistic Quantum Mechanics* (Springer, Heidelberg, 2000).

[31] B. Thaller, *Advanced Visual Quantum Mechanics* (Springer, Heidelberg, 2005).

[32] J. W. Braun, Q. Su, and R. Grobe, Numerical approach to solve the time-dependent Dirac equation, Phys. Rev. A **59**, 604 (1999).

[33] G. R. Mocken and C. H. Keitel, FFT-split-operator code for solving the Dirac equation in 2+1 dimensions, Comput. Phys. Commun. **178**, 868 (2008).

[34] Y. Fu, J. Zeng, and J. Yuan, PCTDSE: A parallel Cartesian-grid-based TDSE solver for modeling laser-atom interactions, Comput. Phys. Commun. **210**, 181 (2017).

[35] A. O. Barut, *Electrodynamics and Classical Theory of Fields and Particles* (Dover, Mineola, NY, 1980).

[36] G. R. Mocken and C. H. Keitel, Quantum dynamics of relativistic electrons, J. Comput. Phys. **199**, 558 (2004).

[37] H. Bauke and C. H. Keitel, Accelerating the Fourier split operator method via graphics processing units, Comput. Phys. Commun. **182**, 2454 (2011).

[38] D. Bauer, P. Mulser, and W.-H. Steeb, Relativistic Ponderomotive Force, Uphill Acceleration, and Transition to Chaos, Phys. Rev. Lett. **75**, 4622 (1995).

[39] G. Casati, B. V. Chirikov, J. Ford, and F. M. Izrailev, *Stochastic Behavior in Classical and Quantum Hamiltonian Systems*, Lecture Notes in Physics Vol. 93 (Springer, Berlin, 1979)

[40] F. L. Moore, J. C. Robinson, C. Bharucha, P. E. Williams, and M. G. Raizen, Observation of Dynamical Localization in Atomic Momentum Transfer: A New Testing Ground for Quantum Chaos, Phys. Rev. Lett. **73**, 2974 (1994).

[41] Y. C. Lai, H. Y. Xu, L. Huang, and C. Grebogi, Relativistic quantum chaos: An emergent interdisciplinary field, Chaos **28**, 052101 (2018).